Werk

Jahr: 1981
Kollektion: fid.geo
Signatur: 8 Z NAT 2148:49
Digitalisiert: Niedersächsische Staats- und Universitätsbibliothek Göttingen
Werk Id: PPN1015067948_0049
PURL: http://resolver.sub.uni-goettingen.de/purl?PPN1015067948_0049

LOG Id: LOG_0056
LOG Titel: Spherical-Earth gravity and magnetic anomaly modeling by Gauss-Legendre Quadrature integration
LOG Typ: article

Übergeordnetes Werk

Werk Id: PPN1015067948
PURL: http://resolver.sub.uni-goettingen.de/purl?PPN1015067948
OPAC: http://opac.sub.uni-goettingen.de/DB=1/PPN?PPN=1015067948

Contact

Niedersächsische Staats- und Universitätsbibliothek Göttingen
Georg-August-Universität Göttingen
Platz der Göttinger Sieben 1
37073 Göttingen
Germany
Email: gdz@sub.uni-goettingen.de

J Geophys (1981) 49:234–242

Journal of Geophysics

Spherical-Earth Gravity and Magnetic Anomaly Modeling by Gauss-Legendre Quadrature Integration

R.R.B. von Frese[1], W.J. Hinze[1], L.W. Braile[1], and A.J. Luca[2]

[1] Department of Geosciences, Purdue University, West Lafayette, Indiana 47907, USA
[2] Chevron Geophysical Co., 400 5th Ave. SW, Calgary, Alberta TPOL7, Canada

Abstract. The usefulness of long-wavelength potential field anomalies in lithospheric interpretation is greatly increased with spherical earth modeling techniques. Gauss-Legendre quadrature integration is used to calculate the anomalous potential of gravity and magnetic fields and their spatial derivatives on a spherical earth for an arbitrary body represented by an equivalent point source distribution of gravity poles or magnetic dipoles. The distribution of equivalent point sources is determined directly from the coordinate limits of the source volume. Variable integration limits for an arbitrarily shaped body are derived from interpolation of points which approximate the body's surface envelope. The versatility of the method is enhanced by the ability to treat physical property variations within the source volume and to consider variable magnetic fields over the source and observation surface. A number of examples verify and illustrate the capabilities of the technique, including preliminary modeling of potential field signatures for Mississippi embayment crustal structure at satellite elevations.

Key words: Spherical coordinate gravity modeling – Spherical coordinate magnetic modeling – Equivalent sources – Gauss-Legendre quadrature integration – Satellite potential fields – Mississippi embayment

Introduction

Computation of theoretical anomalous gravity and magnetic fields from geologic models is an important element in interpreting potential field data and designing surveys. For regional gravity and magnetic surveys measured in degrees of latitude and longitude, procedures are desired which model directly, in spherical coordinates, potential field anomalies due to large-scale, arbitrarily shaped sources of variable density or magnetization characteristics.

In a review of computer modeling techniques Bhattacharyya (1978) presents methods that in principle are suitable for spherical earth modeling of regional features. These procedures are generally based on approximations of the anomalous source as a group of prisms or polygonal laminae, the effects of which are evaluated and summed at each observation point to yield the total anomaly. However, for typical spherical earth modeling applications, the book-keeping problem involved with subdividing the large-scale source into simple forms to reflect arbitrary characteristics of geometry and physical properties is commonly formidable.

A simple and more efficient procedure is to represent quadratures of the source volume by equivalent point sources according to the well known technique of Gaussian quadrature integration. In principle, the appropriate geometric distribution of equivalent point sources can be determined directly from the coordinate limits of the source volume, so that an accurate estimate of the source-affiliated anomaly is obtained by evaluating and summing at each observation point the anomaly values due to each point source of the equivalent source distribution.

Gaussian quadrature is a time-honored technique for numerical integration and has been well studied in the literature of numerical methods (Carnahan et al. 1969). Potential field modeling by Gauss-Legendre quadrature was used by Ku (1977) to evaluate gravity and magnetic anomalies in Cartesian coordinates due to bodies of arbitrary shape and magnetic polarization. In this discussion, the method is extended to spherical coordinates and the general problem of sources with arbitrary shape and variable density and magnetization properties.

Description of Method

As illustrated in Fig. 1, it is convenient for gravity and magnetic modeling problems to consider the anomalous body as being composed of a source volume distribution of gravity point poles or magnetic point dipoles, respectively. Hence, to estimate the anomalous gravity or magnetic field at some observation point, it is necessary to evaluate and sum the anomaly values due to each of these point sources at the observation point.

In particular, the radial anomaly, Δg, due to a gravity point pole referred to a geocentric coordinate system as shown in Fig. 1 is given by

$$\Delta g = \left\{ -G \frac{\partial}{\partial R} \left(\frac{1}{R} \right) \frac{\partial R}{\partial r} \right\} \Delta m \tag{1}$$

where

G = universal gravitational constant ($=6.67 \times 10^{-8}$ cm^3/(g sec^2)),
R = distance from observation point (r, θ, ϕ) to source point (r', θ', ϕ'),
r, r' = radial distances from earth's center to the observation point and source point, repectively,
θ, θ' = co-latitude coordinates of observation and source points, respectively,

0340-062X/81/0049/0234/$01.80

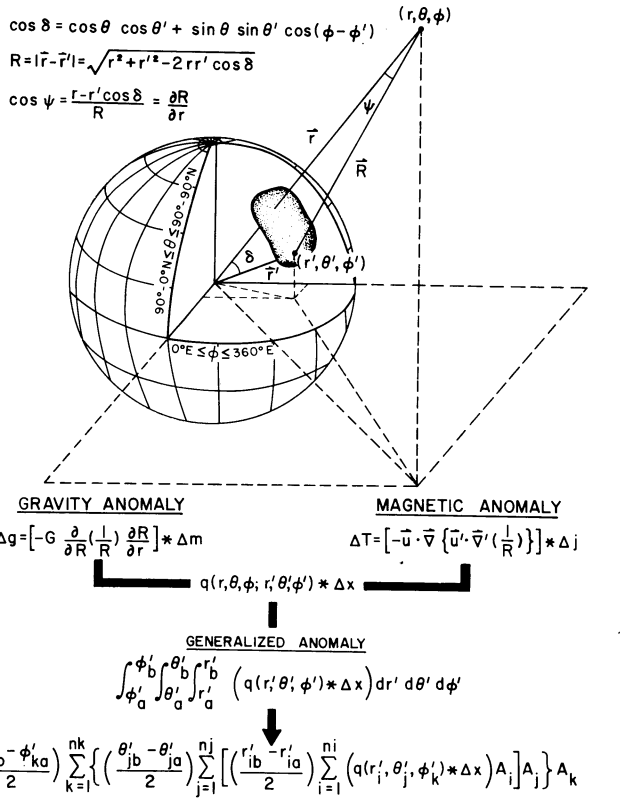

Fig. 1. Gravity and magnetic anomaly modeling in spherical coordinates of a geologic body with arbitrary shape and physical properties by Gauss-Legendre quadrature integration (see text for details)

ϕ, ϕ' = longitude coordinates of observation and source points, respectively, and
Δm = mass contrast of the point pole.

For a magnetic point dipole, on the other hand, the total magnetic intensity anomaly, ΔT, is given by

$$\Delta T = \left\{ -\mathbf{u} \cdot \nabla \left(\mathbf{u}' \cdot \nabla' \left(\frac{1}{R} \right) \right) \right\} \Delta j \tag{2}$$

where

∇, ∇' = gradient operators in observation point and source point coordinates, respectively,
Δj = magnetization contrast of the point dipole, and
$\mathbf{u}, \mathbf{u}'$ = unit geomagnetic field vectors at the observation point and source point, respectively.

Conventionally, the unit vectors $\mathbf{u}$ and $\mathbf{u}'$ are expressed in terms of geomagnetic field inclination (I, I') and declination (D, D'). Also, when the point dipole polarization is by induction

$$\Delta j = \Delta k \, F' \tag{3}$$

where

Δk = magnetic susceptibility contrast of the point dipole, and
F' = scalar geomagnetic field intensity at the source point.

Hence, in regional-scale applications of Eq. (2) geomagnetic field models such as the IGRF-1965 (Cain et al. 1967) are normally used to obtain pertinent values of (I', D', F') at the source point and (I, D) at the observation point.

Consideration of Eqs. (1) and (2) shows that the incremental gravity and magnetic anomaly values due to a point source located a distance R from the observation point can be generalized according to the relation

$$q(R)\,\Delta x \tag{4}$$

where

$q(R)$ = the geometrical point source function which describes the inverse distance between the observation point and source point, and
Δx = the appropriate physical property contrast of the point source.

Hence, to determine the total potential field anomaly it is necessary to evaluate at each observation point (r, θ, ϕ) the volume integral given by

$$\int_{\phi'_a}^{\phi'_b} \int_{\theta'_a}^{\theta'_b} \int_{r'_a}^{r'_b} (q(r, \theta, \phi; r', \theta', \phi')\,\Delta x)\, dr'\, d\theta'\, d\phi' \tag{5}$$

where the primed variables refer to the coordinates of the anomalous body such that

ϕ'_a, ϕ'_b = lower and upper longitude limits of the source volume,
θ'_a, θ'_b = lower and upper co-latitude limits of the source volume, and
r'_a, r'_b = lower and upper radial limits of the source volume.

Consider, now, the numerical evaluation of the innermost integral in Eq. (5). Most numerical integration techniques involve the use of interpolation polynomials to approximate the integrand according to a summation formula of the general type given by

$$\int_{r'_a}^{r'_b} (q(r')\,\Delta x)\, dr' \simeq \sum_{i=1}^{ni} A_i q(r'_i)\,\Delta x \tag{6}$$

where the ni values A_i are the weights to be given to the ni functional values $(q(r'_i)\,\Delta x)$ evaluated at the interpolation coordinates, r'_i. Conventional integration formulae such as Simpson's rule or the trapezoidal rule assume equal spacing of the arguments r'_i which is generally appropriate when dealing with an integrand that is not well known analytically. However, as shown in Eqs. (1) and (2) the integrand being considered here involves a familar analytic function which may be computed for any argument to great precision. In such instances, Gaussian quadrature formulae can be developed to yield selected values of interpolation r'_i and coefficients A_i so that the sum in Eq. (6) gives the integral exactly when $(q(r')\,\Delta x)$ is a polynomial of degree $2ni$ or less (Carnahan et al. 1969).

In general, it may be shown that the Gaussian coefficients A_i can be obtained from a polynomial of order ni which is orthogonal over the interval of integration such that the ni points of interpolation r'_i are the zeros of the polynomial. Families of orthogonal polynomials which are commonly used to develop Gaussian quadrature formulae include Legendre, Laguerre, Chebyshev and Hermite polynomials. However, in this discussion, only the prototype of the Gaussian method involving Legendre polynomials is considered.

Legendre polynomials $P_{ni}(\bar{r})$ of order ni which are orthogonal over the interval $-1 \leq \bar{r} \leq 1$ are given by

$$P_{ni}(\bar{r}) = \left(\frac{1}{2^{ni}\, ni!} \right) \left(\frac{d^{ni}}{d\bar{r}'^{ni}} (\bar{r}'^2 - 1)^{ni} \right), \quad \text{where } P_0(\bar{r}') = 1 \tag{7}$$

Accordingly, the standard Gauss-Legendre quadrature over the interval $(-1, 1)$ is given by

$$\int_{-1}^{1} (q(\bar{r}')\,\Delta x)\,d\bar{r}' \simeq \sum_{i=1}^{ni} A_i q(\bar{r}'_i)\,\Delta x \tag{8}$$

where the interpolation points $\bar{r}'_i$ at which the integrand is evaluated are the zeros of Eq. (7) and the Gaussian coefficients are

$$A_i = \frac{2(1-\bar{r}'^2_i)}{ni^2\{P_{ni-1}(\bar{r}'_i)\}^2} \tag{9}$$

Now for arbitrary limits of integration such as indicated in Eq. (6) it is necessary to map the standard interval $-1 \leqq \bar{r}'_i \leqq 1$ into the interval of integration $r'_a \leqq r'_i \leqq r'_b$ according to the transformation

$$r'_i = \frac{\bar{r}'_i(r'_b - r'_a) + (r'_b + r'_a)}{2} \tag{10}$$

Accordingly, the integral in Eq. (6) can be approximated as

$$\int_{r'_a}^{r'_b} (q(r')\,\Delta x)\,dr' = \frac{(r'_b - r'_a)}{2} \int_{-1}^{1} \left(q\left\{ \frac{\bar{r}'_i(r'_b - r'_a) + (r'_b + r'_a)}{2} \right\} \Delta x \right) dr'$$

$$\simeq \frac{(r'_b - r'_a)}{2} \sum_{i=1}^{ni} A_i q(r'_i)\,\Delta x \tag{11}$$

Extending this procedure to volume integrals is straightforward. Thus, the Gauss-Legendre formula for the general evaluation of Eq. (5) is given by

$$\int_{\phi'_a}^{\phi'_b} \int_{\theta'_a}^{\theta'_b} \int_{r'_a}^{r'_b} (q(r', \theta', \phi')\,\Delta x)\,dr'\,d\theta'\,d\phi' \simeq \left(\frac{\phi'_{kb} - \phi'_{ka}}{2}\right) \sum_{k=1}^{nk} \left\{ \left(\frac{\theta'_{jb} - \theta'_{ja}}{2}\right) \times \sum_{j=1}^{nj} \left\{ \left(\frac{r'_{ib} - r'_{ia}}{2}\right) \sum_{i=1}^{ni} (q(r'_i, \theta'_j, \phi'_k)\,\Delta x)\,A_i \right\} A_j \right\} A_k \tag{12}$$

where

$$r'_i = 0.5\,\{\bar{r}'_i(r'_{ib} - r'^a_{ia}) + r'_{ib} + r'_{ia}\}$$
$$\theta'_j = 0.5\{\bar{\theta}'_j(\theta'_{jb} - \theta'_{ja}) + \theta'_{jb} + \theta'_{ja}\}$$
$$\phi'_k = 0.5\,\{\bar{\phi}'_k(\phi'_{kb} - \phi'_{ka}) + \phi'_{kb} + \phi'_{ka}\}$$

$\bar{r}'_i, \bar{\theta}'_j, \bar{\phi}'_k$ = coordinates of the subdivision in the limits of integration from -1 to 1 which correspond to zero nodes of Eq. (7),

A_i, A_j, A_k = Gauss-Legendre quadrature coefficients given by Eq. (9),

ϕ'_{ka}, ϕ'_{kb} = lower and upper longitude limits of the body for the k-th longitude component of the equivalent point source coordinates,

$\theta'_{ja}, \theta'_{jb}$ = lower and upper co-latitude limits of the body for the j-th co-latitude component of the equivalent point source coordinates, and

r'_{ia}, r'_{ib} = lower and upper radial limits of the body for the i-th radial component of the equivalent point source coordinates.

The quadrature formula given in Eq. (12) shows that gravity and magnetic anomalies can be computed accurately by summing at each observation point the anomalous effect of $nk \times nj \times ni$ equivalent point sources located at source point coordinates $(r'_i, \theta'_j, \phi'_k)$, where each of the differential point source anomalies is appropriately weighted by Gauss-Legendre quadrature coefficients and the volume coordinate limits of the anomalous body being modeled. This result is well suited to machine computation where the input consists principally of values of the integrand for selected source points $(r'_i, \theta'_j, \phi'_k)$, affiliated subdivision coordinates $(\bar{r}'_i, \bar{\theta}'_j, \bar{\phi}'_k)$, and coefficients (A_i, A_j, A_k), and the volume coordinate limits of the body for each dimension of every source point coordinate $(r'_i, \theta'_j, \phi'_k)$.

The selected values of the integrand for gravity or magnetic modeling purposes are readily obtained from Eqs. (1) or (2), respectively. Also, the Legendre subdivision coordinates of the interval $(-1, 1)$ and associated Gaussian coefficients may be computed directly from Eqs. (7) and (9), respectively. However, it is generally found to be more machine efficient to input these values from tables using an algorithm such as described by Carnahan et al. (1969). Values which are applicable for such algorithms are tabulated to 30 digit precision for orders $n = 2$–512 by Stroud and Secrest (1966). However, for most regional lithospheric modeling applications experience suggests that subdivision coordinates and associated coefficients to 10 digit precision for orders up to $n = 16$ are normally sufficient.

For a uniformly dimensioned body such as a prism, the integration limits for the evaluation of Eq. (12) are easy to specify. In this case, for example, $(\phi'_{ka}, \phi'_{kb}) = (\phi'_a, \phi'_b)$, $(\theta'_{ja}, \theta'_{jb}) = (\theta'_a, \theta'_b)$ and $(r'_{ia}, r'_{ib}) = (r'_a, r'_b)$. However, for the more general case of a body with arbitrary shape the integration limits are known in one dimension only, so that the problem of determining the integration limits in the remaining two dimensions for each equivalent point source coordinate must be considered.

Procedures can be developed to handle this problem efficiently, such as the method described by Ku (1977) where a modified cubic spline function is used to interpolate the desired integration limits from a set of body point coordinates which provide a rough approximation of the surface envelope of the body. Typically, the procedure is to specify, for example, the longitudinal limits of integration of the body to obtain the nk Gauss-Legendre nodes ϕ'_k as described above. Interpolations of the body point coordinates are performed next to determine the maximum and minimum latitude coordinates of the body for each longitude coordinate ϕ'_k. These values of course provide the latitude limits of integration for evaluating the nj nodes θ'_j. Similarly, the radial coordinates of the body points are interpolated at each horizontal coordinate (ϕ'_k, θ'_j) to yield appropriate radial limits of integration from which the ni nodes r'_i can be determined. Procedures such as this are readily adapted for efficient machine processing so that the integration limits of arbitrarily shaped bodies can be determined accurately for evaluation of the quadrature formula given in Eq. (12).

The quadrature formula in general has considerable versatility in modeling applications because anomalous gravity and magnetic potentials and their respective spatial derivatives of any order are all linearly related. Hence, to model the radial derivative of the potential field anomaly due to an arbitrary source, for example, it is necessary simply to exchange $q(R)$ for $\partial q(R)/\partial r$ in Eq. (12). Additional geophysically interesting quantities which can be modeled from simple linear transformations of the integrand of Eq. (12) include the anomalous potential, vector anomaly components and the spatial derivatives of any order. Relative geoidal anomalies can also be modeled by computing the anomalous gravitational potential of the body at the surface of the earth and dividing it by normal gravity according to Brun's formula (Heiskanen and Moritz 1967).

Bodies with variable physical property contrast are also accommodated readily by the quadrature solution. To emphas-

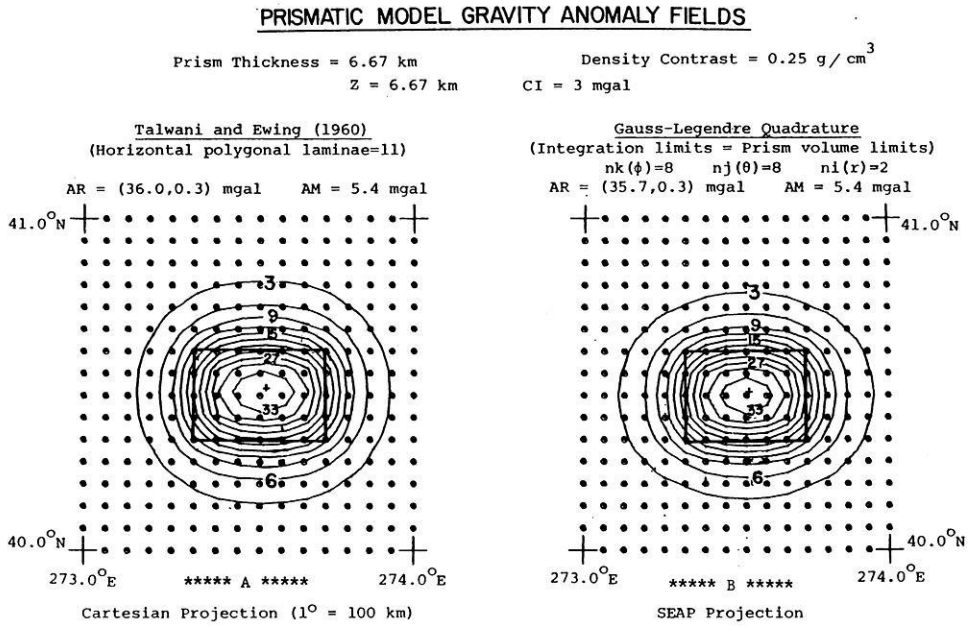

Fig. 2. Gravity anomaly comparisons for a spherical prism

ize the fact that Δx can be expressed as a function of source position (i.e., $\Delta x = \Delta x(r', \theta', \phi')$) when necessary, the generalized point source anomaly $(q(R)\,\Delta x)$ has been carried intact throughout the foregoing developments. Conventional modeling procedures normally assume bodies with uniform physical properties so that each property variation must be modeled as a separate body. To model the total intensity magnetic anomaly due to a regional source subject to regional variations of geomagnetic field induction by the well known method of Talwani (1965), for example, requires that the source be subdivided into blocks wherein the geomagnetic field polarization is uniform. Each block in turn must be subdivided into a group of approximating polygonal laminae to ensure accuracy of the numerical integration which evaluates the anomaly. By contrast, the Gauss-Legendre quadrature approach is simply to polarize each point dipole in the quadrature formula according to the polarization characteristics of an acceptable numerical model of the geomagnetic field (e.g., the IGRF-1965 by Cain et al. 1967). This example also illustrates the technique for modeling bodies with remanent magnetization by quadrature formulation. Here, the magnetization of the point dipoles is achieved using a polarization field that represents the vector sum of induced and remanent magnetic polarizations.

Finally, considerable computational flexibility is available for the practical implementation of the quadrature formulation. Ku (1977) noted the trade-offs which occur in applications of the method between efficient computation and the accuracy of the solution. A large number of Gauss-Legendre nodes ensures a very accurate quadrature solution, although the same degree of accuracy can often be achieved by a substantially smaller number of equivalent point sources. In fact, the accuracy of the solution remains essentially unchanged for different numbers of nodes as long as the node spacing is smaller than the distance to the observation point. Hence, the minimum number of nodes specified in a given application should be such that the distance to the observation point is greater than the node spacing. In general, then, the accuracy of the quadrature formulation can be readily controlled by adjusting the number of Gauss-Legendre nodes relative to the elevation of the observation point.

Illustration of Method

A computer program is described in von Frese et al. (1980) which was developed for regional lithospheric gravity and magnetic modeling applications by Gauss-Legendre quadrature. The program was used to construct examples that illustrate some of the capabilities of the method.

To demonstrate and verify the method for regional-scale modeling applications, gravity and magnetic anomalies due to a three-dimensional spherical prism were modeled on a spatial scale small enough that the results could be compared readily with conventional modeling techniques in Cartesian coordinates. In Fig. 2, for example, a comparison is made between the two coordinate systems for calculations of gravity anomalies due to a 6.67 km thick prism with density contrast 0.25 g/cm^3. The observation grid consists of (16,16) stations uniformly spanning the region (273–274) °E, (40–41) °N at an elevation (Z) of 6.67 km above the top of the prism.

The well known method of Talwani and Ewing (1960) was used to calculate the gravity effect of the prismatic model as shown in Fig. 2A. The gravity anomaly was determined by evaluating and summing at each observation point the gravity anomalies due to 11 horizontal polygonal laminae used to approximate the prism. As shown in Fig. 2A, the resultant anomaly has an amplitude range (AR) between 36.0 mgal and 0.3 mgal and an amplitude mean (AM) of 5.4 mgal. The anomaly was computed and contoured in Cartesian coordinates assuming $1° = 100$ km. This assumption distorts slightly the true geometry of a spherical prism in this $1° \times 1°$ region in northwestern Indiana where 1° in longitude or latitude is more nearly equal to 88 km or 112 km, respectively.

In Fig. 2B the gravity anomaly of the spherical prism computed by Gauss-Legendre quadrature integration is contoured on a stereographic equal-area polar (SEAP) projection. In this case, the gravity anomaly was calculated in spherical coordinates by evaluating at each observation point an $nk \times nj \times ni = 8 \times 8 \times 2 = 128$ point quadrature formula where the integration limits were specified directly from the spherical coordinate limits of the prism volume. The results shown in Fig. 2 indicate that the two methods agree very well with respect to

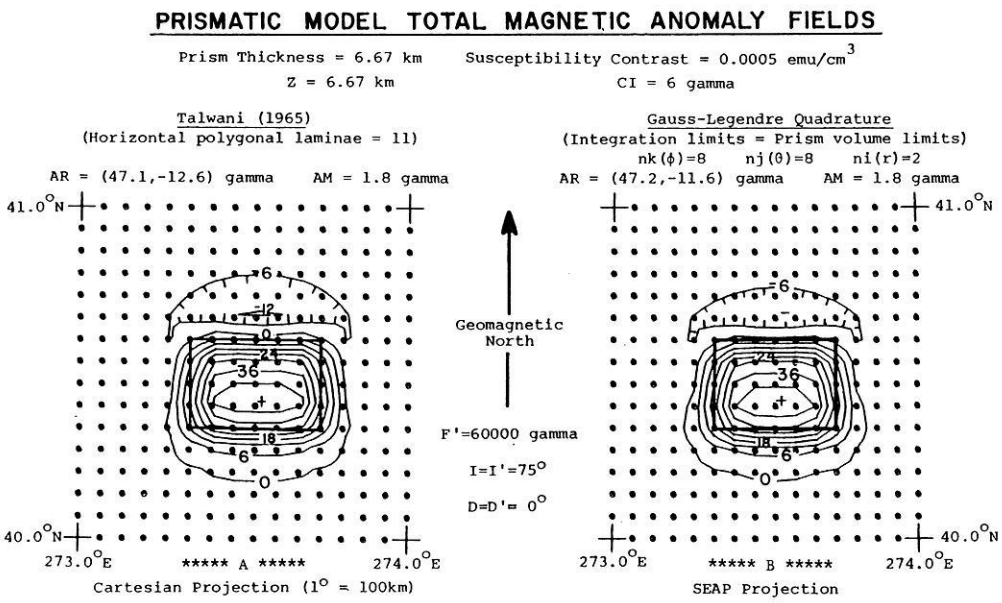

Fig. 3. Magnetic anomaly comparisons for a spherical prism

the relatively small spatial scale under consideration. The slight disparity between the results is probably due to geometric distortion introduced by the use of Cartesian coordinates for calculation of the spherical prism anomaly.

A comparison of magnetic anomaly fields is illustrated in Fig. 3 for the prism model with volume magnetic susceptibility contrast equal to 0.0005 emu/cm^3 ($4\pi \times 0.0005$ in SI units) and uniform polarizing intensity $F' = 60{,}000$ gamma (60,000 nT), inclination $I' = 75°$ and declination $D' = 0°$. Over the observation grid, uniform geomagnetic field attitude characteristics of inclination $I = 75°$ and declination $D = 0°$ are also assumed. The total intensity magnetic anomaly of the spherical prism calculated in Cartesian coordinates according to the method of Talwani (1965) is shown in Fig. 3A. The resultant anomaly corresponds well with the magnetic anomaly calculated in spherical coordinates by Gauss-Legendre quadrature in Fig. 3B.

As a more regional-scale example, consider the application of Gauss-Legendre quadrature integration for modeling gravity and magnetic anomaly signatures, at the satellite elevation of 450 km, due to the crustal thickness anomaly which is gridded in Fig. 4A. This zone of enhanced crustal thickness, extending from the Texas panhandle northeastward into Kansas, is portrayed by seismic evidence (Warren and Healy 1973) as roughly 10 km of lighter crustal material displacing denser (mantle) material to a depth of 50 km. To illustrate the gravity modeling procedure, a density contrast of -0.3 g/cm^3 was assumed for this feature.

Magnetic considerations, on the other hand, suggest that the crustal thickness anomaly may represent a zone of positive magnetization contrast due to downward deflection of the Curie isotherm in the region of thick, cooler crustal material or thicker magnetic crust extending into non-magnetic mantle material. For the purposes of this example, a volume susceptibility contrast of 10^{-2} emu/cm^3 was assumed for the zone of enhanced crustal thickness which is representative of the general magnetization reported for the lower crust (Hall 1974; Shuey et al. 1973).

To determine the variable limits of integration for the evaluation of the quadrature formula, the crustal thickness anomaly was referred to the body point grid shown in Fig. 4A. For each Gauss-Legendre node in the ϕ'-longitude coordinates of the body, the θ'-latitude limits of the body were interpolated from the 6 points describing the body's boundary. The radial limits, in turn, were interpolated from the 6 boundary points and 3 interior points of the body for each Gauss-Legendre node with horizontal (ϕ', θ')-coordinates. For the particular model considered here, of course, the radial coordinates of the 9 body points used to approximate the subsurface configuration of the body were specified to represent a uniform thickness of 10 km.

The resultant gravity anomaly at 450 km elevation due to this feature is illustrated in Fig. 4B. The gravity effect was calculated by evaluating an $nk \times nj \times ni = 16 \times 16 \times 2 = 512$ point Gauss-Legendre quadrature formula over the (41, 41) grid of observations. The magnetic effect of the crustal thickness anomaly was also computed in this manner at 450 km elevation. The resultant total intensity magnetic anomaly in the 1GRF-1965 updated to 1968 is demonstrated in Fig. 5A. To remove anomaly distortion due to regional variability of the reference field, the magnetic effect was next computed, assuming a uniform polarizing field intensity of 60,000 gamma and radial geomagnetic field inclination at both source and observation points. Accordingly, Fig. 5B illustrates the resultant magnetic anomaly field reduced to radial polarization at 450 km elevation for the crustal thickness model.

Finally, for accurate implementation of the method the distance between the equivalent source points and the observation point must be greater than the equivalent source point spacing within the body. This limitation can be minimized in practice by either subdividing the body into an appropriate number of smaller bodies, or increasing the number of equivalent point sources, or increasing the distance between the observation point and the body. The latter consideration suggests that the Gauss-Legendre quadrature formulation is especially well suited for modeling satellite-level gravity and magnetic anomalies because of the large elevations involved with these measurements. The gravity and magnetic anomaly signatures of the crustal thickness model, for example, can be computed using an $nk \times nj \times ni = 4 \times 4 \times 2 = 32$ point quadrature formula to nearly the same precision as developed by the 512 point formula in Fig. 4B and 5, respectively.

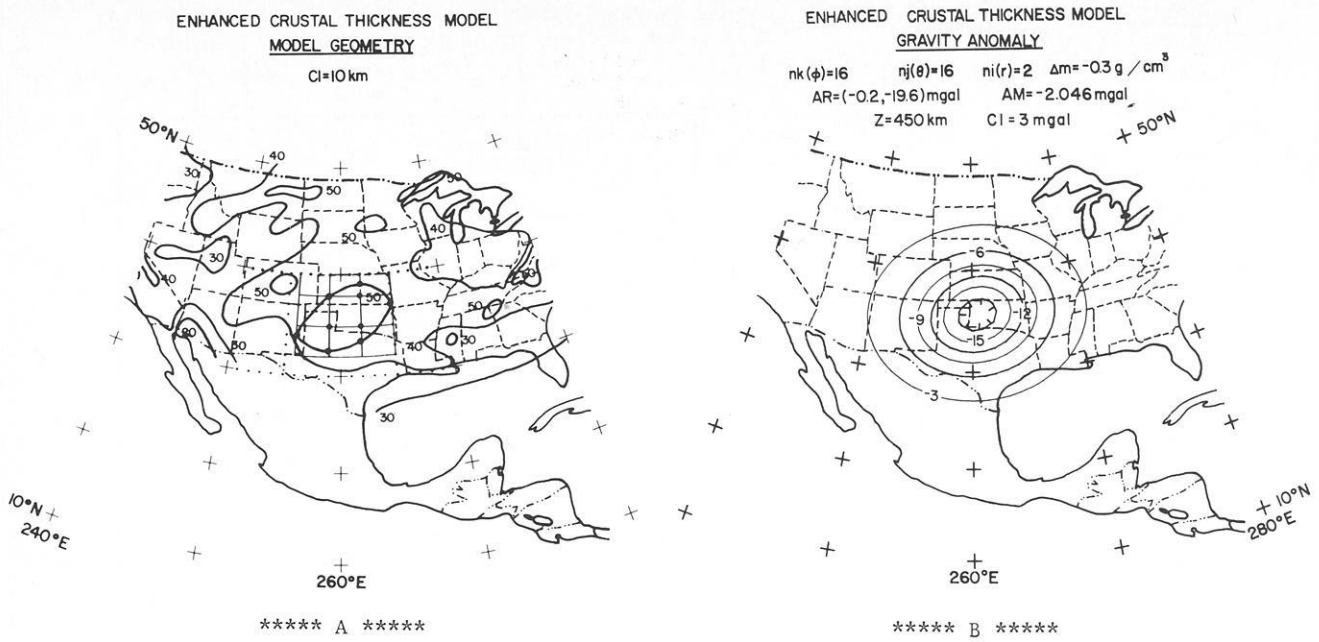

Fig. 4. A SEAP projection of crustal thickness anomaly model geometry adapted from Warren and Healy (1973). The model is referred to a body point grid which gives latitude, longitude, and top and bottom radial coordinates for the 9 points of the model's surface envelope used to interpolate the variable volume limits of integration. The shape of the thickened crust (10 km) is indicated by the 50 km depth contour on which the grid is superimposed. **B** SEAP projection of the gravity anomaly for the crustal thickness model calculated at 450 km elevation by Gauss-Legendre quadrature integration

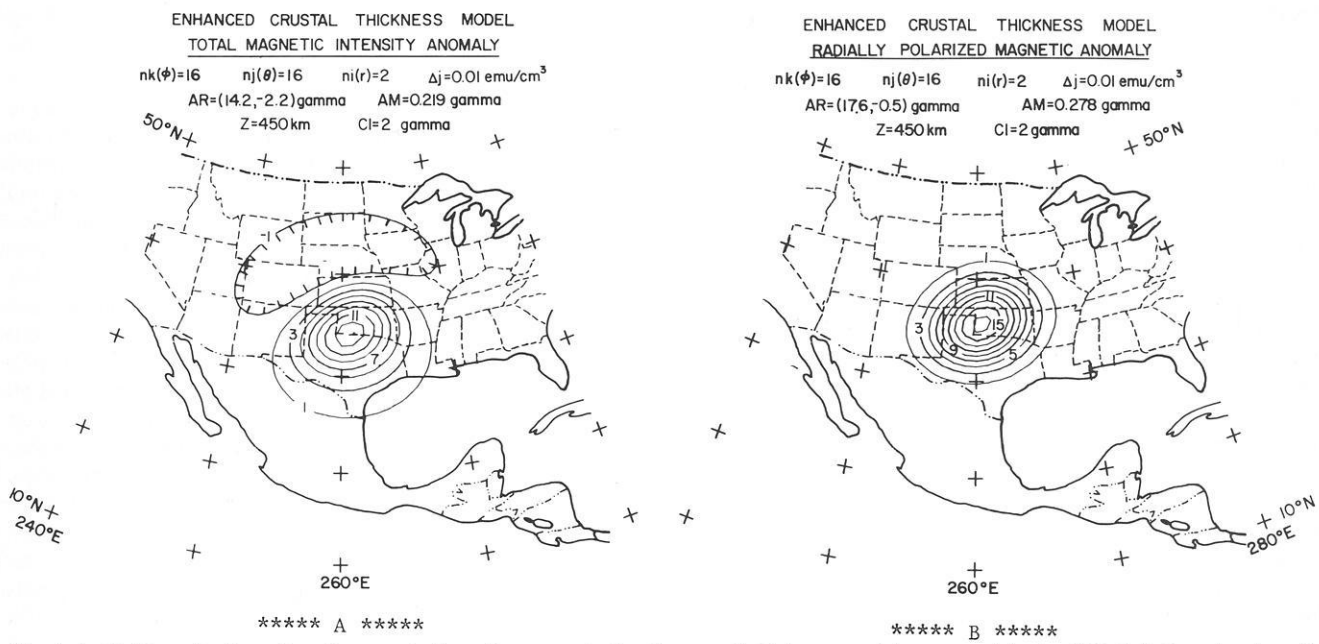

Fig. 5. A SEAP projection of total magnetic intensity anomaly for the crustal thickness model computed in the IGRF-1965 updated to 1968 by Gauss-Legendre quadrature integration. **B** SEAP projection of reduced-to-the-pole magnetic anomaly for the crustal thickness model by Gauss-Legendre quadrature integration using a normalized polarizing amplitude of 60,000 gamma

Application of Method

The spherical earth modeling procedure was used to obtain a preliminary view of the gravity and magnetic anomaly characteristics for the Mississippi embayment at 450 km elevation. This information is pertinent to evaluating, for example, the feasibility of using satellite gravity and magnetic surveys for detecting anomaly signatures due to failed rifts.

The Mississippi embayment represents a broad, spoon-shaped re-entrant of Mesozoic and Cenozoic sedimentary rocks which extends into the Paleozoic terrain of the North American craton from the south as outlined by the shaded contour of Fig. 6D. The axis of this feature roughly parallels the Mississippi River tapering northward into the tectonically active region of the New Madrid seismic zone. An integrated analysis of gravity, seismic, stratigraphic and petrologic data by Ervin

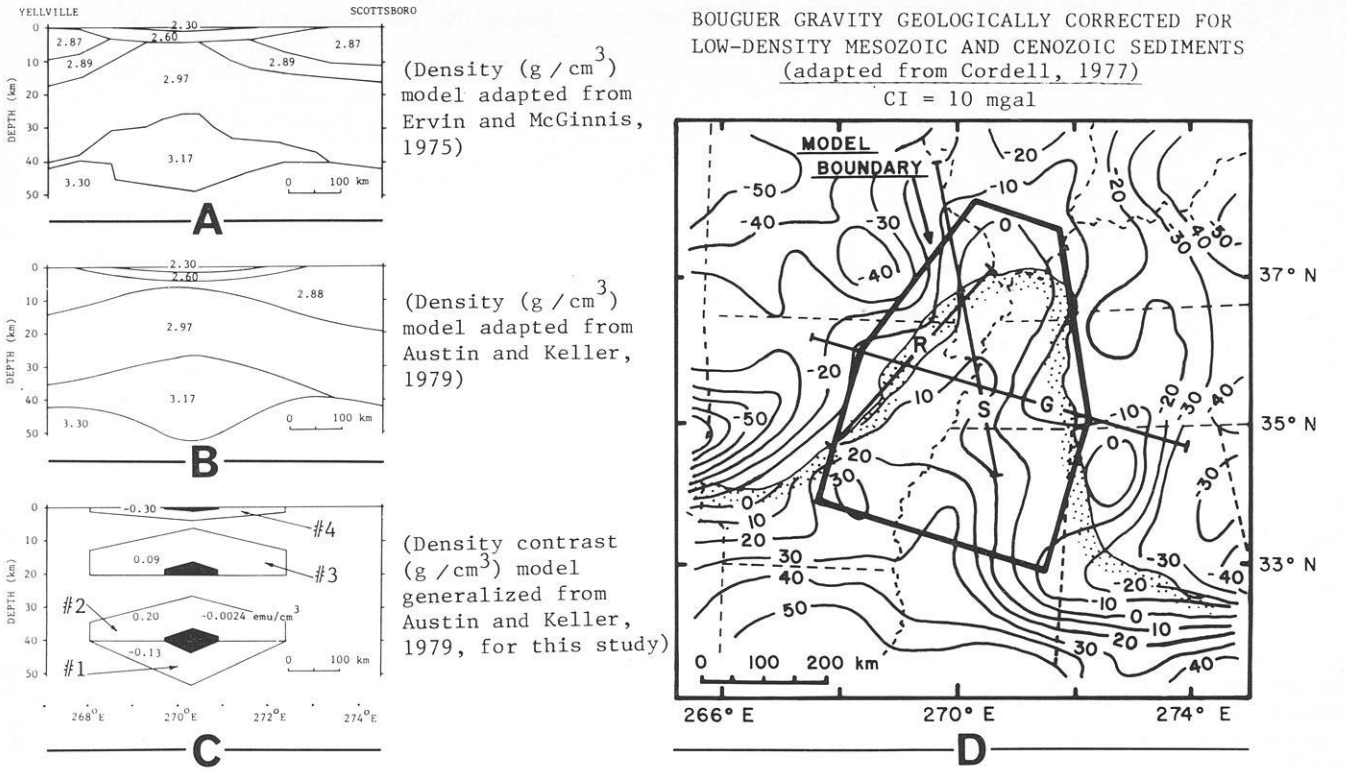

Fig. 6A–D. Development of Mississippi embayment density and magnetization models. Also shown in (**D**) is an index map of the embayment (*shaded contour*) where *G* is the gravity profile studied by Ervin and McGinnis (1975), *R* is the seismic refraction line studied by McCamy and Meyer (1965), and *S* is the surface wave propagation path studied by Austin and Keller (1979)

and McGinnis (1975) suggests the embayment is a late Precambrian aulacogen which was reactivated most recently in the late Cretaceous by tensional forces initiated during the formation of the present Atlantic ocean basin by subsidence of the Gulf coastal plain.

Figure 6A is a cross-section of the density structure of the Mississippi embayment given by Ervin and McGinnis (1975) along a profile between Yellville, Arkansas and Scottsboro, Alabama (hereafter called $Y-S$ profile). This density model was synthesized from regional gravity data derived from the U.S. Bouguer gravity anomaly map of Woollard and Joesting (1964) and the results of a reversed seismic refraction profile between Little Rock, Arkansas and Cape Girardeau, Missouri as described by McCamy and Meyer (1966). Austin and Keller (1979) integrated the work of McCamy and Meyer (1966) with an analysis of Rayleigh wave dispersion along a propagation path between Oxford, Mississippi and Florissant, Missouri to obtain a similar density model for the $Y-S$ profile which is illustrated in Fig. 6B. An index map for locating these various studies is given in Fig. 6D. In general, the crustal cross-sections shown in Fig. 6A, B support the failed-rift model for the origin of the Mississippi embayment.

The agreement of surface wave, seismic refraction, and gravity data in the region of the embayment suggests that the crustal cross-section given in Fig. 6B can be useful for developing a reasonably valid three-dimensional model of the embayment. Accordingly, the crustal cross-section that was generalized from Fig. 6B for the purposes of this study is given as the four-body model shown in Fig. 6C. The gravity analysis due to Cordell (1977) was used to project the characteristics of this generalized crustal cross-section north and south of the $Y-S$ profile.

Cordell (1977) corrected the smoothed positive Bouguer anomaly of the embayment for the low-density sediments and observed the long continuous positive anomaly with an amplitude of 15–45 mgal increasing southward illustrated in Fig. 6D. The axis of this anomaly closely follows the Mississippi River northward beyond its confluence with the Ohio River into southern Illinois. The anomaly exhibits relatively uniform behavior south of the $Y-S$ profile until about 33° N where it increases sharply, thus suggesting that the crustal cross-section may be uniformly projected southward along the Mississippi River to approximately 33° N. To the north, decreasing gravity anomaly values in conjunction with the northward tapering surface configuration of the embayment suggest a commensurate northward tapering projection of the crustal cross-section along the Mississippi River into southern Illinois. Hence, to obtain the first-order, three-dimensional generalization of the crustal structure of the embayment used in this investigation, the crustal cross-section of Fig. 6C was projected uniformly south of the $Y-S$ profile and tapered uniformly northward as outlined in Fig. 6D. The northern ends of the four bodies of this generalized model as projected onto the cross-section along the $Y-S$ profile are given by the shaded regions of Fig. 6C.

To compute the potential field anomalies at 450 km elevation, each of the four bodies of this generalized model was represented by a Gauss-Legendre quadrature formula consisting of 128 equivalent point sources. The latitude and longitude limits of each body were represented by 8 point sources and the radial limits by 2 point sources. Pertinent body volume limits were interpolated from a set of body points that sampled the coordinates of the surface envelope for each body. The quadrature formulae were next evaluated and summed over a (21, 13) observation grid spanning the region (260–280) °E, (33–

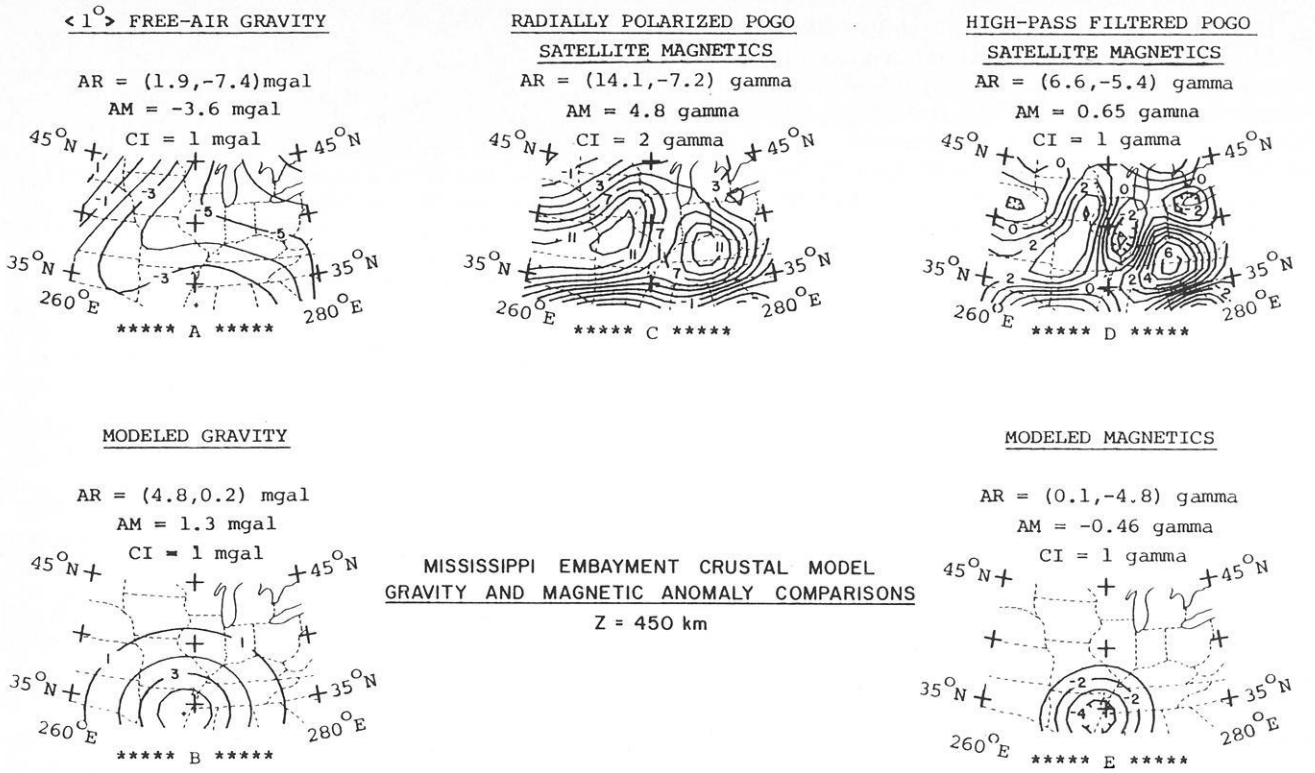

Fig. 7A–E. Mississippi embayment satellite-level comparisons between Gauss-Legendre quadrature modeled gravity and magnetic anomalies and upward continued 1°-averaged free-air gravity and reduced-to-the-pole POGO satellite magnetic anomaly data. Each anomaly field is plotted on a stereographic equal-area polar projection

45) °N and compared to observed gravity and magnetic anomaly data at 450 km elevation.

Upward continuation of free-air gravity anomaly values from the surface of the earth to an elevation of 450 km by equivalent point source inversion for the study area leads to the results shown in Fig. 7A. These data exhibit a pronounced relative positive anomaly with slightly greater than 3 mgal of relative amplitude in the region of the embayment. The gravity effect of the generalized four-body model described above is shown in Fig. 7B as roughly a 4 mgal anomaly. The general agreement between the modeled and observed data over the embayment suggests that the observed gravity anomaly can be reasonably well accounted for at 450 km elevation by the generalized four-body model.

Polar Orbiting Geophysical Observatory (POGO) satellite magnetometer observations reduced to radial polarization using a normalization amplitude of 60,000 gamma by equivalent point source inversion are given for the study area in Fig. 7C. These data show a prominent east-west magnetic high that is breached in the vicinity of the embayment by a magnetic low. To give better resolution of the characteristics of the magnetic anomaly for the embayment region, the radially polarized data were high-pass filtered for anomaly wavelengths smaller than about 10°. The high-pass filtered data are illustrated in Fig. 7D and show a negative anomaly of roughly −3 gamma over the embayment.

Wasilewski et al. (1979) found that most analyses of medium to long-wavelength magnetic anomalies suggest that sources are probably contained in the lower crust which, in general, may be substantially more magnetic than the upper crust. The conditions for coherent regional magnetization are enhanced as crustal depth increases. Remanence and thermal overprints are diminished, and viscous magnetization and initial susceptibility are enhanced with increasing temperature especially within 100°–150° C of the Curie point. The thickness of the crust within this thermal regime may be 5–20 km depending on the steepness of the geothermal gradient. Accordingly, they suggest that deep crustal magnetic sources are probably related to lateral variations of petrologic factors or Curie isotherm topography.

Accordingly, an obvious deep crustal source for the observed magnetic anomaly is body #2 (Fig. 6C) which also represents the major gravity source of the embayment model. Austin and Keller (1979) propose that the combination of bodies #1 and #2 was formed as a manifestation of a mantle upwarp beneath the embayment comprising of a mixture of crust and upper mantle material which subsequently cooled to form a block of high density material. Magnetic hypotheses which are consistent with this view include body #2 as a zone of negative magnetization contrast with respect to the lower crust due to depletion of magnetic minerals. Negative magnetization for body #2 also can result from temperatures which exceed the Curie point, although present heat flow data (Sass et al. 1976) do not appear to warrant this hypothesis for the embayment.

Body #3 may represent an additional magnetic source for the embayment assuming crustal magnetization increases with depth. However, the positive magnetic contribution of body #3 will be relatively weak if the Curie isotherm depth is about 40 km or more. Arguments for including bodies #1 and #4 in a magnetic model of the embayment appear to be lacking, so that body #2 probably represents the primary source for the observed magnetic anomaly data if the Curie isotherm is at about 40 km of depth in the region of the embayment.

Hence, the magnetic anomaly due to body #2 was calculated in Fig. 7E using a magnetization contrast of -2.4×10^{-3} emu/cm^3. These results show that the anomaly amplitude observed for the region of the embayment at 450 km elevation can be matched well by a source such as body #2 located near the base of the crust with magnetic properties which correspond with the magnetization characteristics anticipated for the lower crust. Substantial disparity is apparent, however, when the spatial characteristics of the observed and modeled magnetic anomalies are compared. Further refinements of the magnetic model are necessary and will be particularly warrented when data are available from the current Magsat program (Langel 1979) to verify and further upgrade the POGO satellite magnetic anomalies for lithospheric applications. Accordingly, body #2 as determined by gravity modeling considerations represents only a preliminary magnetic model for the embayment.

Conclusions

Regional gravity and magnetic anomaly modeling for arbitrarily shaped lithospheric sources with variable physical properties can be achieved accurately and efficiently in spherical coordinates using Gauss-Legendre quadrature integration. The procedure involves representation of the anomalous source as a distribution of equivalent point gravity poles or point magnetic dipoles which contribute incremental anomaly values evaluated and summed at each observation point to obtain the total anomaly. The distribution of equivalent point sources is determined directly from the volume limits of the anomalous body. For an arbitrarily shaped body, the variable limits of integration can be obtained from interpolations performed on a set of body points which approximate the surface envelope of the anomalous source.

A chief practical advantage of the method is its considerable versatility. The physical properties of the equivalent point sources, for example, can be individually varied to reflect physical property variations of the body being modeled. The method can also be readily extended to model the geoidal anomaly, vector components, and spatial derivatives to any order of the body's anomalous gravitational and magnetic potentials. Finally, the accuracy of the method can be controlled by adjusting the number of equivalent point sources or the distance between the source and observation point. In this regard, the method is particularly well suited for satellite gravity and magnetic anomaly modeling because the efficiency and accuracy of the application increases with increasing distance between source and observation points.

In consideration of the foregoing results, it is concluded that Gauss-Legendre quadrature integration facilitates a powerful and efficient approach to spherical earth modeling of regional-scale lithospheric gravity and magnetic anomaly sources. Accordingly, the method has widespread application in the analysis and design of regional-scale gravity and magnetic surveys for lithospheric investigation.

Acknowledgements. Financial support for this investigation was provided by the Goddard Space Flight Center under NASA Contract NAS5-25030.

References

Austin, C.B., Keller, G.R.: A crustal structure study of the Mississippi Embayment. In: An integrated geophysical and geological study of the tectonic framework of the 38th parallel lineament in the vicinity of its intersection with the extension of the New Madrid fault zone, U.S. Nuclear Regulatory Commission Rept. NUREG/CR-1014, Braile, L.W., Hinze, W.J., Sexton, J.L., Keller, G.R., Lidiak, E.G., eds: 101–133, 1979

Bhattacharyya, B.K.: Computer modeling in gravity and magnetic interpretation. Geophysics **43**, 912–929, 1978

Cain, J.C., Hendricks, S.J., Langel, R.A., Hudson, W.V.: A proposed model for the International Geomagnetic Reference Field, 1965. J. Geomagn. Geoelectr. **19**, 335–355, 1967

Carnahan, B., Luther, H.A., Wilkes, J.O.: Applied Numerical Methods. New York: J. Wiley and Sons, Inc. 1969

Cordell, L.: Regional positive gravity anomaly over the Mississippi Embayment. Geophys. Res. Lett. **4**, 285–287, 1977

Ervin, C.P., McGinnis, L.D.: Reelfoot rift: Reactivated precursor to the Mississippi Embayment. Geol. Soc. Am. Bull. **86**, 1287–1295, 1975

Frese, R.R.B. von, Hinze, W.J., Braile, L.W., Luca, A.J.: Spherical earth gravity and magnetic anomaly modeling by Gauss-Legendre quadrature integration. NASA Rept NAS5-25030, 1980

Hall, D.H.: Long-wavelength aeromagnetic anomalies and deep crustal magnetization in Manitoba and Northwestern Ontario, Canada. Pageoph. **40**, 403–430, 1974

Heiskanen, W.A., Mortiz, H.: Physical Geodesy. San Francisco: W.H. Freeman and Co. 1967

Ku, C.C.: A direct computation of gravity and magnetic anomalies caused by 2- and 3-dimensional bodies of arbitrary shape and arbitrary magnetic polarization by equivalent point method and a simplified cubic spline. Geophysics **42**, 610–622, 1977

Langel, R.A.: Near-earth satellite magnetic field measurements: A prelude to Magsat. EOS (Trans. Am. Geophys. Union) **60**, 667–668, 1979

McCamy, K., Meyer, R.P.: Crustal results of fixed multiple shots in the Mississippi Embayment; In: The Earth Beneath the Continents, Steinhart, J.S., Smith, T.J., eds: Am. Geophys. Union Geophys. Monogr. **19**, 370–381, 1966

Sass, J.H., Diment, W.H., Lachenbruch, A.H., Marshall, B.V., Munroe, R.J., Moses, T.H., Jr., Urban, T.C.: A new heat-flow contour map of the conterminous United States. U.S.G.S. Open-file Rept. 76–756, 1976

Shuey, R.T., Schellinger, D.K., Johnson, E.H., Alley, L.B.: Aeromagnetics and the transition between the Colorado Plateau and the Basin and Range Provinces. Geology **1**, 107–110, 1973

Stroud, A.H., Secrest, D.: Gaussian Quadrature Formulas. New Jersey: Prentice-Hall 1966

Talwani, M., Ewing, M.: Rapid computation of gravitational attraction of three-dimensional bodies of arbitrary shape. Geophysics **25**, 203–225, 1960

Talwani, M.: Computation with the help of a digital computer of magnetic anomalies caused by bodies of arbitrary shape. Geophysics **30**, 797–817, 1965

Warren, D.H., Healy, J.H.: Structure of the crust in the conterminous United States. Tectonophysics **20**, 203–213, 1973

Wasilewski, P.J., Thomas, H.H., Mayhew, M.A.: The Moho as a magnetic boundary, NASA Rept. NASA-GSFC TM80245, 1979

Woollard, G.P., Joesting, H.R.: Bouguer gravity anomaly map of the United States. Am. Geophys. Union and U.S. Geological Survey, scale 1:2,500,000, 1964

Received July 29, 1980
Accepted January 15, 1981

J Geophys (1981) 49:243–244

Journal of Geophysics

Short Communication

Detection Probabilities for Earthquakes in Sweden

A. Shapira, O. Kulhánek, and R. Wahlström
Seismological Department, Box 12019, S-750 12 Uppsala, Sweden

Key words: Detection probability – Earthquakes in Sweden – Swedish Seismograph Station Network – Threshold magnitude – Weak regional seismic events

In recent years, the need for improved seismic risk evaluations in Sweden has led to accurate estimates of detection probabilities with respect to weak Swedish earthquakes. Generally, these rather low-magnitude events ($M_L < 4$) are recorded only by means of the *Swedish Seismograph Station Network* (SSSN), currently consisting of six permanent stations. Only occasionally do neighbouring Finnish and/or Norwegian stations also contribute with arrival-time readings. Hence, for weak regional events, we lack the usual reference system of organisations like ISC, NEIS or EMSC when estimating the detection performance of the SSSN-stations. The problem has recently been studied and a solution suggested by Shapira et al. (1979a), to be referred to as Paper I. In short, their method, which is based upon a modification of the approach of Ringdal (1975), enables the estimation of threshold magnitudes for weak events monitored exclusively by regional networks.

The main objective of the present short communication is to indicate the ability of the SSSN to detect earthquakes in Sweden and the relative detection contributions from individual network stations. The data used comprise 121 earthquakes located within Sweden and adjacent waters (Wahlström 1978). The statistical model used and other theoretical aspects of the modified approach are discussed in greater detail in Paper I and are not repeated here.

When applying the modified approach, the detectability is related to the epicentral distance rather than to a certain seismic region. To introduce the distance dependence, all available earthquakes are relocated to a common epicentral distance. It is assumed that recorded amplitudes and periods are not influenced by performing the distance and corresponding magnitude conversion. Employment of the distance transformation enables calculations of magnitudes for fictitious events located at a number of chosen epicentral distances. For more details, the reader is referred to Paper I and to Shapira et al. (1979b).

The decision "detected" or "not detected" is based upon the conserved amplitude and period values linked with the *Sg*-phase. Thus, when the actual earthquake is detected by station *A*, then it is assumed that all relocated events associated with this actual earthquake, are also detected. The percentage of detections, for each magnitude, is fitted to the detection curve $P(M_R)$ which yields estimates of biased threshold magnitudes $b \pm s$. Corrected threshold magnitudes $\hat{b} = b + C_A$ and their variance $\hat{s}^2 = s^2 - \rho_A^2$ are to be used when comparing the detecting power of stations within the network. C_A is station magnitude bias and ρ_A^2 is magnitude variance.

The modified approach has been applied to each of the six SSSN-stations. Events were relocated to a common epicentral distance of 500 km. A fit to the detection curve and estimates of b and s, associated with 50% probability, are presented in Fig. 1 Numerical values of $\hat{b}$ and $\hat{s}$, corresponding to 50% probabilities, are also given in Fig. 1. Considering 90% detection levels, station UDD contributes to the detecting power more than any other station of the SSSN. The second best station is SKA, although its operational magnification is the lowest among the six stations.

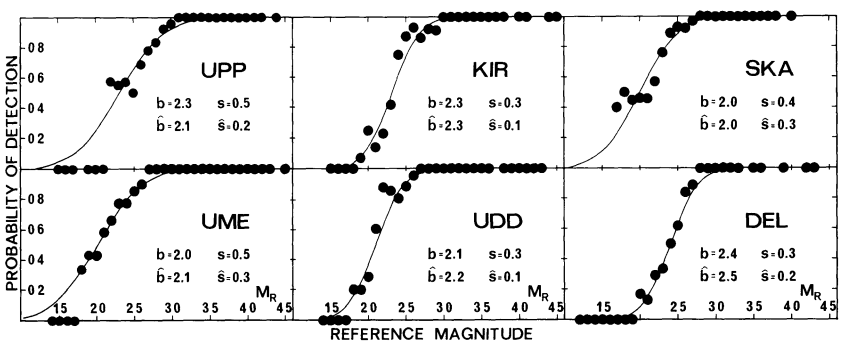

Fig. 1. Matched detection curves, $P(M_R)$ (*solid lines*), and observed detection probabilities (*solid circles*) for the six stations considered (*UPP* = Uppsala, *KIR* = Kiruna, *SKA* = Skalstugan, *UME* = Umeå, *UDD* = Uddeholm, *DEL* = Delary) and for epicentral distance of 500 km. Biased and corrected threshold magnitudes and corresponding variances, associated with 50% probabilities, are given for each station

0340-062X/81/0049/0243/$01.00